

Supplementary Materials:

A Fault Slip Transient on the North Anatolian Fault

Baptiste Rousset¹, Romain Jolivet², Mark Simons³, Cécile Lasserre¹, Bryan Riel³,
Pietri Milillo^{3,4}, Ziyadin Cakir⁵ and Francois Renard¹

¹ ISTerre, Université Grenoble Alpes, CNRS, IRD, Grenoble, France

² Laboratoire de Géologie, Département de Géosciences, École Normale Supérieure, PSL Research University, CNRS UMR 8538, Paris, France

³ Seismological Laboratory, Geological and Planetary Sciences, California Institute of Technology, Pasadena, California, USA.

⁴ School of Engineering, University of Basilicata, 85100 Potenza, Italy

⁵ Department of Geology, Istanbul Technical University, Istanbul, Turkey

1 Supplementary materials: InSAR data and time series analysis reveal a transient episode of creep

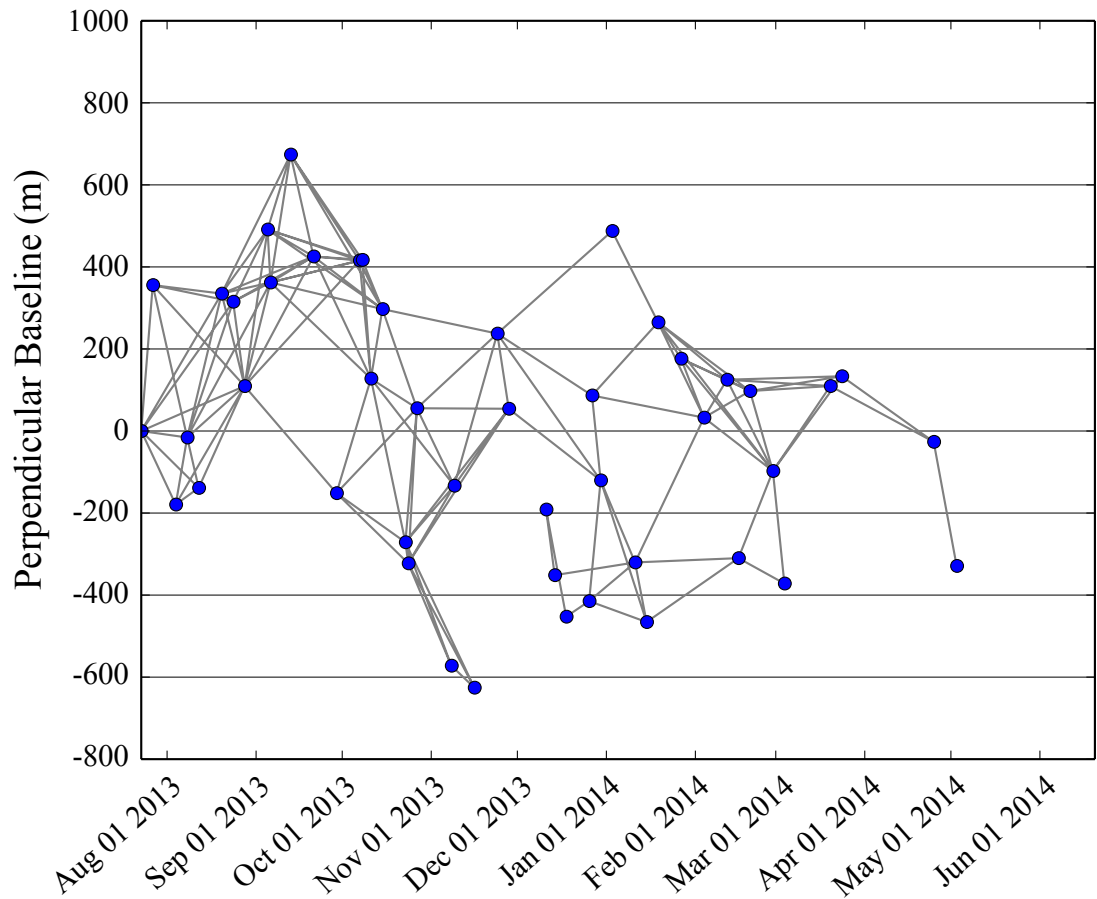


Figure S1: **Perpendicular baseline versus time of the ascending SAR acquisitions (Fig. 1).** Blue dots correspond to the acquisitions and grey lines to the interferograms used in this study. Interferograms not computed are incoherent near the fault zone.

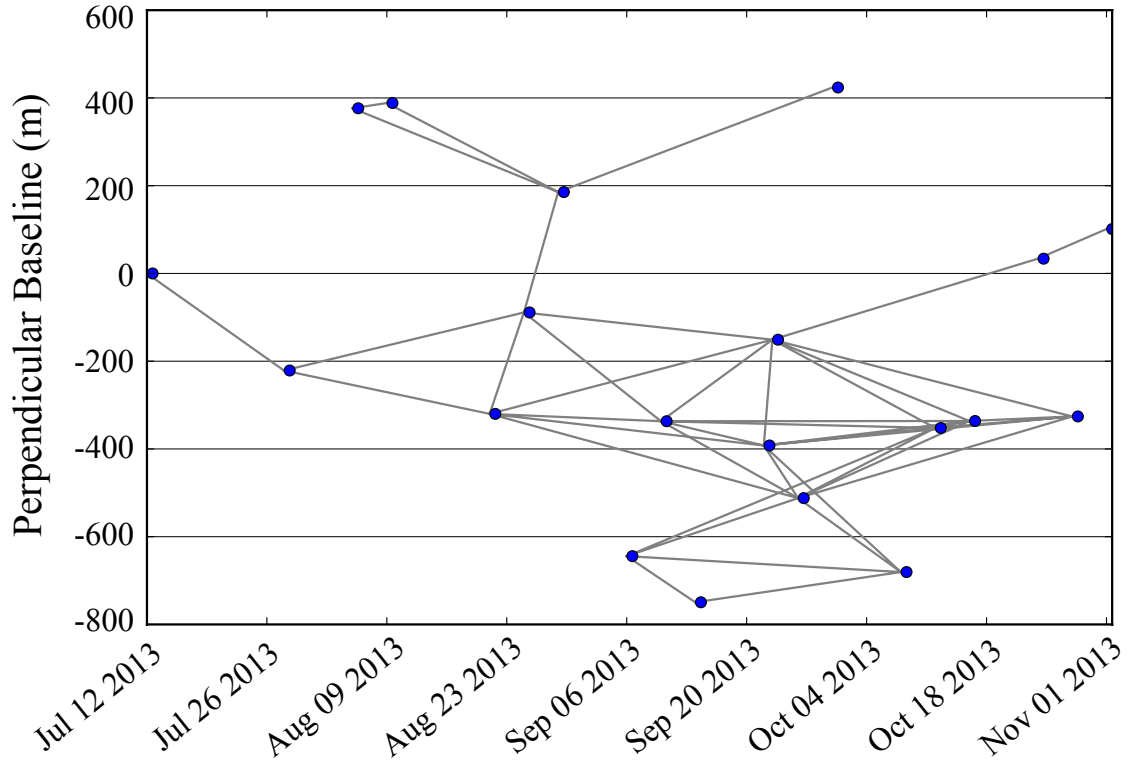


Figure S2: **Perpendicular baseline versus time of the descending SAR acquisitions (Fig. 1).** Blue dots correspond to the acquisitions and grey lines to the interferograms used in this study. Interferograms not computed are incoherent near the fault zone.

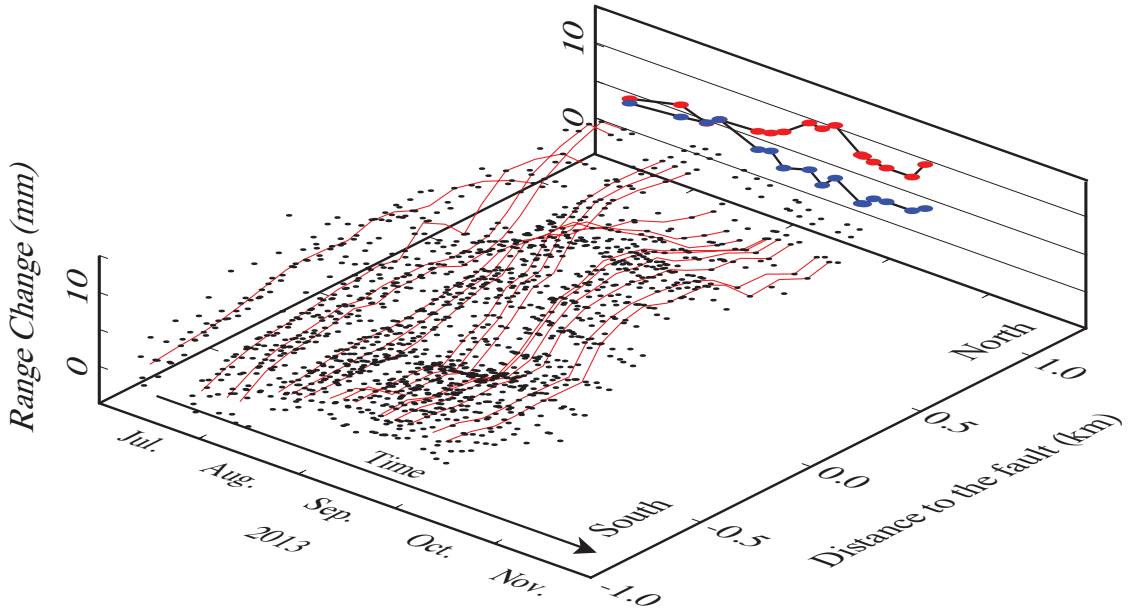


Figure S3: **Profiles of surface LOS displacement perpendicular to the NAF as a function of time (Same as Fig. 3 of the main text but for the descending track).** The plot shows the temporal evolution between July 2013 and November 2013 of surface LOS displacement on a 500 m wide and 2 km long profile centered on the fault. Blue (south) and red (north) dots curves show average range change taken from two 100-m-wide swaths located 300 m apart from each others on each side of the fault.

2 Supplementary materials: Slip distribution of the creep burst

Table 1: Elastic properties of the lithosphere used to build the Green's functions in a stratified medium, with the ratio $Vp/Vs = 1.75$.

Depth (km)	$\mu(GPa)$	$V_p (km.s^{-1})$	density ($kg.m^{-3}$)
0	14.1	4.00	2700
5	24.5	5.00	3000
13	34.2	5.91	3000
20	36.5	6.10	3000
25	40.1	6.40	3000
36	61.1	7.90	3000
90	70.7	8.10	3300

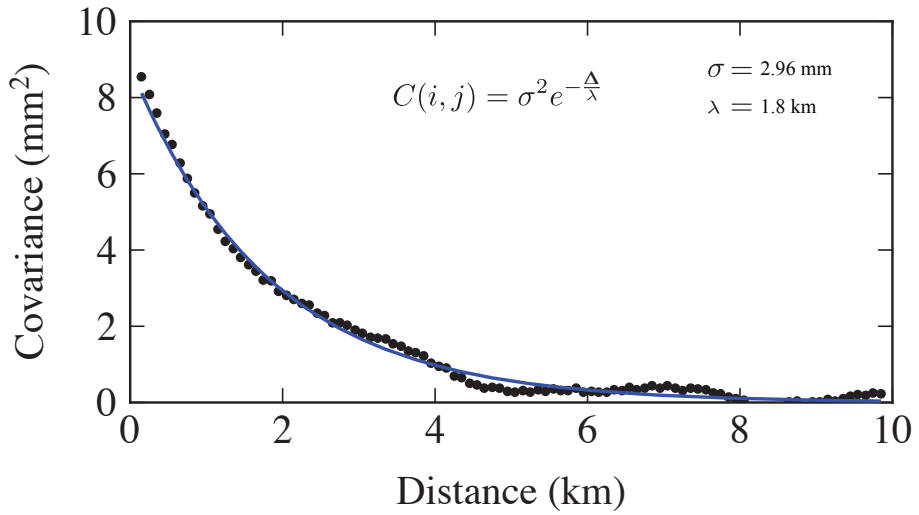


Figure S4: **Data covariance.** One-dimensional empirical covariance and best exponential fit based on the approach used in Jolivet et al. (2012). The covariance $C(i,j)$ between two pixels i and j is given by $C(i,j) = \sigma^2 e^{-\frac{\Delta}{\lambda}}$. σ corresponds to the amplitude of the covariance, and λ to the characteristics correlation length of the covariance. Δ is the distance between pixels i and j .

Constrained least square model

As it is commonly used in the fault modelling community, we show that it is possible to get a model close to the mode of the posterior PDF presented in the main text using a constrained least square approach. However, we want to note that the prior model and the smoothing are here tuned so that the model corresponds to the mode of the posterior PDF without justification for this choice of parameters. For the unique model presented, we solve for slip using a regularized least-square approach, whereby we minimize the cost function $S(\mathbf{m})$ that is the sum of the L2 norm of the residuals and of the difference between our model and a prior model ([Tarantola, 2005](#)):

$$S(\mathbf{m}) = \frac{1}{2}(\mathbf{d} - \mathbf{G}\mathbf{m})^T \mathbf{C}_d^{-1}(\mathbf{d} - \mathbf{G}\mathbf{m}) + \frac{1}{2}(\mathbf{m} - \mathbf{m}_0)^T \mathbf{C}_m^{-1}(\mathbf{m} - \mathbf{m}_0), \quad (1)$$

where, \mathbf{m}_0 is our prior model (here, the null vector) and, in a Bayesian sense, the center of the prior PDF of the model. \mathbf{C}_m is the model covariance matrix, describing the width of the prior PDF and the correlation between the parameters in our prior assumption. We use an exponential function to describe the model covariance \mathbf{C}_m ([Jolivet et al., 2012](#); [Radiguet et al., 2012](#)),

$$\mathbf{C}_m = \sigma_m^2 e^{-\frac{\Delta}{\lambda}} \quad (2)$$

where σ_m is the standard deviation of the model parameters and λ is the correlation length. For the slip distribution presented in Figure S5, we arbitrarily chose a σ_m of 30 mm and a correlation length λ of 4 km and only consider positive slip values (i.e. slip cannot be left-lateral). We minimise the cost function using the Sequential Least Square Programming implementation of the Scipy python library.

In this particular model, slip corresponding to the surface creep burst is constrained between the surface and a depth of 5 km, with a peak slip of 2.3 cm at the surface. Slip extends for about 8 km along strike, leading to an equivalent moment of 1.2e17 N.m (Mw 5.3).

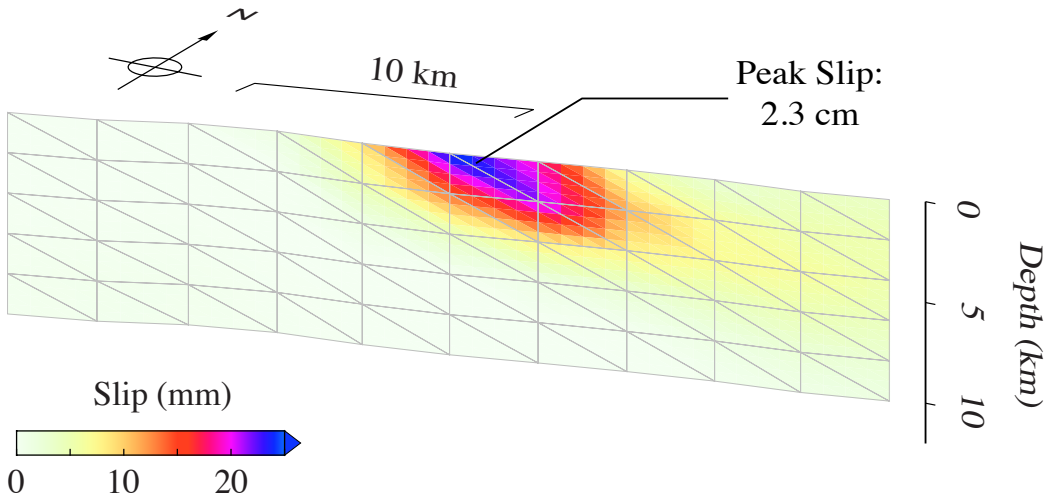


Figure S5: Slip distribution for a smoothed constrained least square slip inversion. Smoothing is imposed using an exponential covariance in the space of the models with a characteristic length scale of 4 km and a prior model at zero slip. Note that with such a parametrisation of the smoothing, the slip repartition is similar to the one of the mode of the posterior PDF (Fig. 4 of the main text).

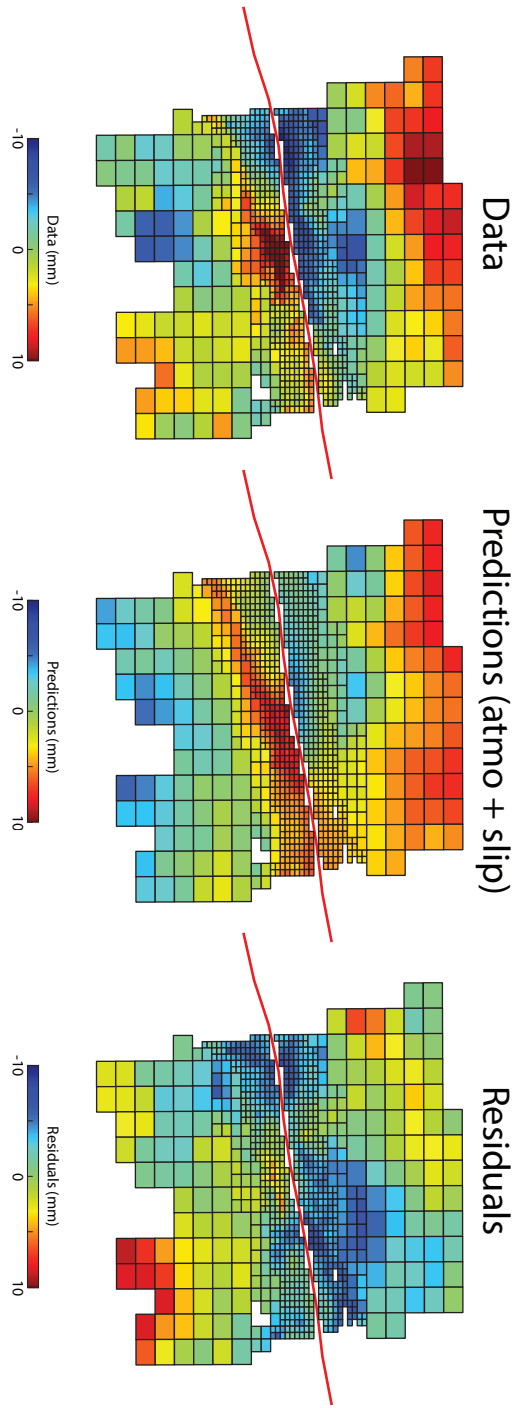


Figure S6: Comparison between data and model from the Bayesian inversion.
 Left: Down-sampled data used for the inversion. Note that the downsampling is made using the method described in Lohman and Simons (2005). Middle: Modelled displacements in the LOS corresponding to the mode of the posterior PDFs accounting both for the slip on the fault and the atmospheric signal linearly correlated with the topography. Right: Residuals between the left and middle panels.

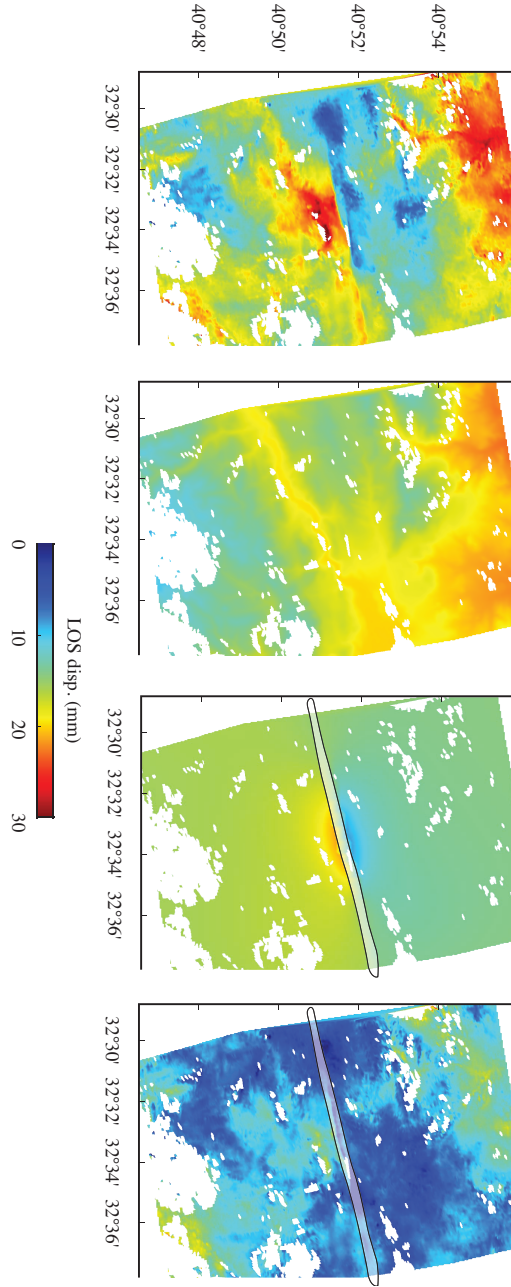


Figure S7: Data compared to the two terms of the model at full resolution. Left: Data used at full resolution. Middle left: Mode of the posterior PDF corresponding to the linear term correlated to the topography. Middle right: Surface displacement corresponding to the mode of strike slip on the discretised fault interface. Note that the surface pattern of displacement does not extend far from the fault trace because of the slip shallowness. Right: residuals between the left panel and the sum of the two middle ones. Pixels in the shaded area are excluded from the inversion as they lie too close to the modeled fault (<200m).

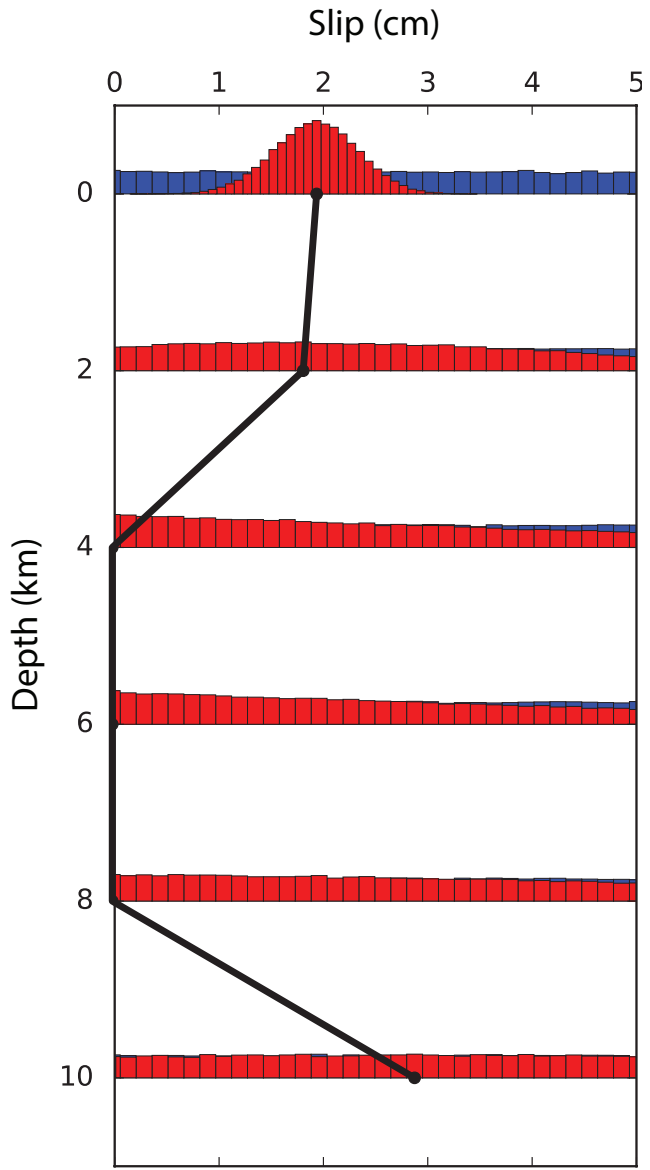


Figure S8: Slip as a function of depth at the middle of the creep burst. The blue and red histograms correspond to the prior and the posterior density functions of slip, respectively. The black curve links the modes of posterior PDF at each depths. At the surface, the posterior PDF has a well defined Gaussian shape, while at lower depths they are Dirichelet like, indicating a lack of resolution. However, the repartition of modes indicates that the slip is likely to not extend at depths higher than 4 km.

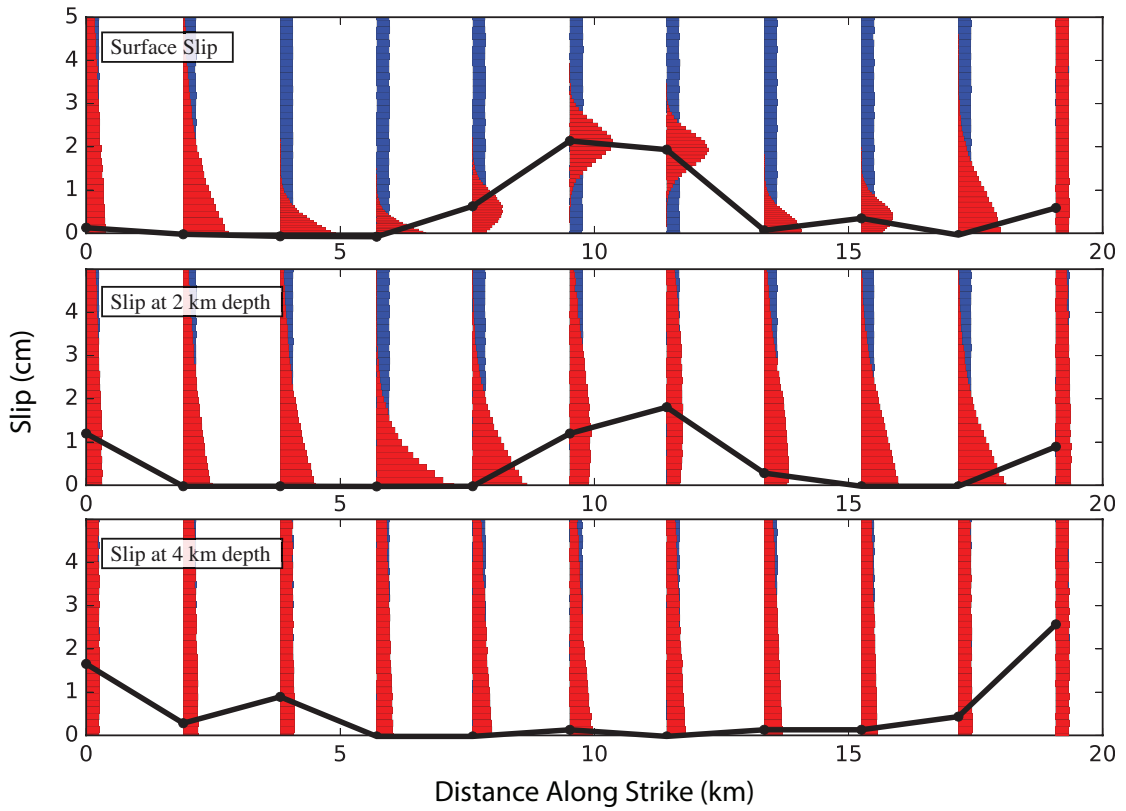


Figure S9: Slip as a function of distance along strike and depth. Same as figure S8 but for several points along the fault trace, extending 10 km to each side of the point of maximum of creep. At the surface, PDFs are concentrated and suggests that slip extends horizontally over 8 km. No slip is observed at depths greater than 4 km.

3 Supplementary materials: Discussion

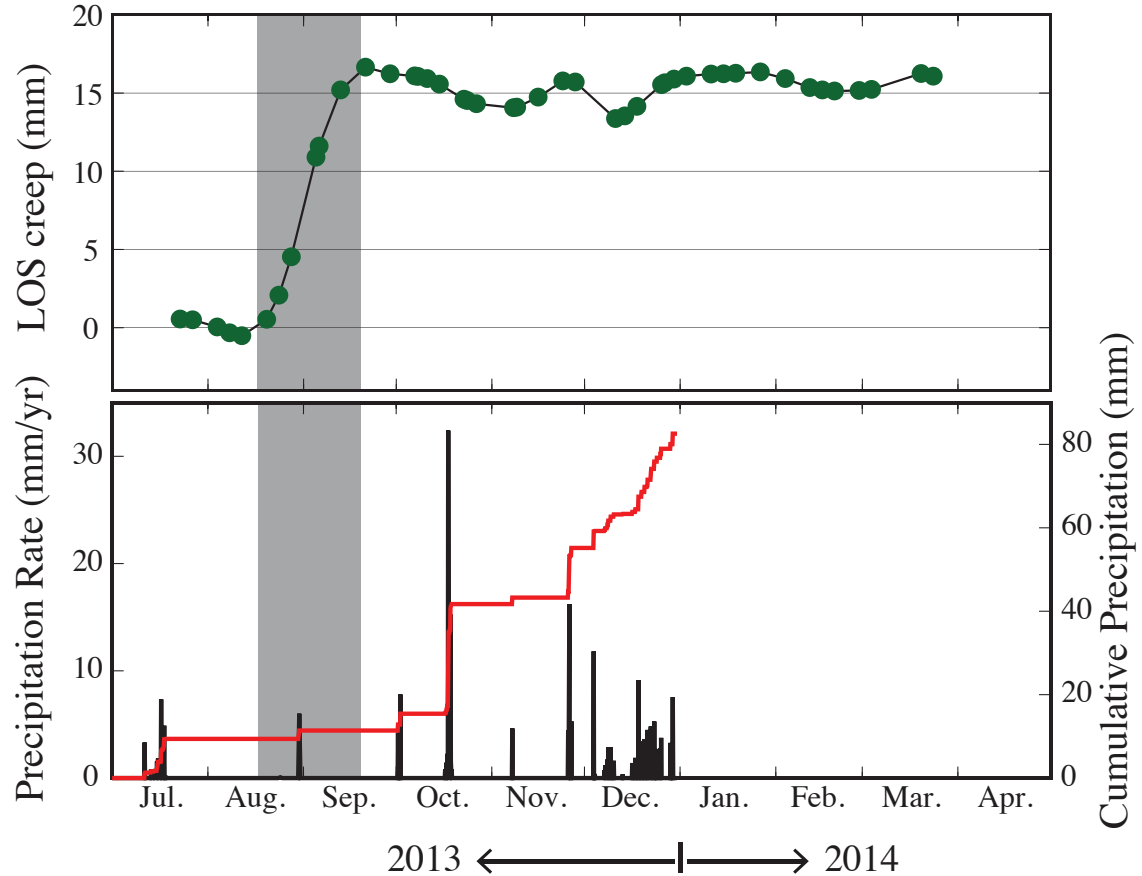


Figure S10: **Comparison between precipitations and the creep burst.** Top: Temporal evolution of the LOS component of surface fault creep. The creep burst is highlighted in grey. Bottom: Precipitation rate and cumulative precipitation in the area of the creep burst. The measurement of precipitations is made by the Tropical Rainfall Measuring Mission (TRMM) satellite ([Simpson et al., 1996](#)). Note that no precipitation is recorded just before the creep burst.

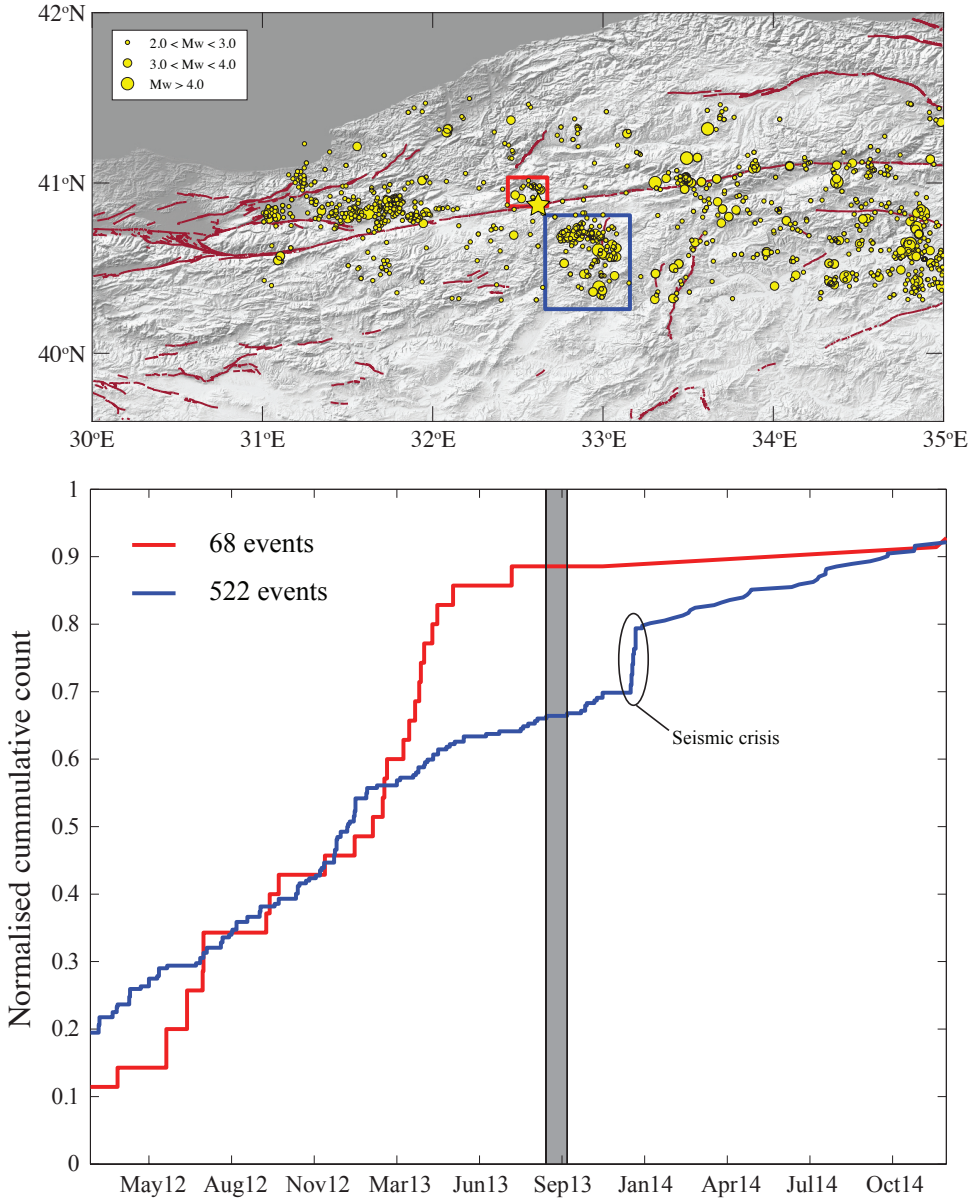


Figure S11: Comparison between the local seismicity and the creep burst. Top: Map with all local seismic events in yellow from March 2012 to December 2014 (Personal communication from Hyrullah Karabulut). Events of magnitudes from 2.0 to 3.0, 3.0 to 4.0 and higher than 4.0 are distinguished by different circle sizes. The geologically mapped fault traces are in burgundy. The location of the creep burst is represented by a yellow star. Bottom: Normalised cumulative count for seismic events located in the red and blue boxes on top. The creep burst is indicated by the grey rectangle. Events located in the red box are almost all Mw 2.5 events and are located at the location of an open mine and are thus probably explosions due to the mine extraction. These events ceased in June 2013. We note the December 2013 seismicity crisis in region shown by the blue box. However, no clear event is identifiable to have dynamically triggered the creep burst.

References

- Jolivet, R., Lasserre, C., Doin, M.-P., Guillaso, S., Peltzer, G., Dailu, R., Sun, J., Shen, Z.-K., and Xu, X. (2012). Shallow creep on the Haiyuan fault (Gansu, China) revealed by SAR interferometry. *J. Geophys. Res.*, 117(B6):401.
- Lohman, R. B. and Simons, M. (2005). Some thoughts on the use of InSAR data to constrain models of surface deformation: Noise structure and data downsampling. *Geochem. Geophys. Geosys.*, 6(Q01):006.
- Radiguet, M., Cotton, F., Vergnolle, M., Campillo, M., Walpersdorf, A., Cotte, N., and Kostoglodov, V. (2012). Slow slip events and strain accumulation in the Guerrero gap, Mexico. *J. Geophys. Res.*, 117(B4).
- Simpson, J., Kummerow, C., Tao, W.-K., and Adler, R. F. (1996). On the tropical rainfall measuring mission (TRMM). *Meteorology and Atmospheric physics*, 60(1-3):19–36.
- Tarantola, A. (2005). *Inverse problem theory and methods for model parameter estimation*. Society for Industrial & Applied.